Original Article

Characterization of the xeno-GVHD response generated by advanced lung cancer patient peripheral blood mononuclear cells in NSG-SGM3 mice

Vered Fuchs[1#], Laila Roisman[2#], Maha Msamra[1], Yael Refaely[3], Aharon Yehonatan Cohen[4], Angel Porgador[1], Nir Peled[2], Ariel Sobarzo[1,5]

[1]The Shraga Segal Department of Microbiology, Immunology, and Genetics, Faculty of Health Sciences, Ben-Gurion University of the Negev, Beer Sheva, Israel; [2]Helmsley Cancer Center, Shaare Zedek Medical Center, Jerusalem, Israel; [3]Department of Cardiothoracic Surgery, Soroka University Medical Center, Beer-Sheva, Israel; [4]The Oncology Institute, Soroka University Medical Center, Beer-Sheva, Israel; [5]The Preclinical Research Center, Faculty of Health Sciences, Ben-Gurion University of the Negev, Beer-Sheva, Israel

Contributions: (I) Conception and design: N Peled, A Sobarzo, L Roisman, V Fuchs; (II) Administrative support: AY Cohen, Y Refaely; (III) Provision of study materials or patients: N Peled, L Roisman; (IV) Collection and assembly of data: V Fuchs, M Msamra, A Sobarzo; (V) Data analysis and interpretation: V Fuchs, A Sobarzo; (VI) Manuscript writing: All authors; (VII) Final approval of manuscript: All authors.

[#]These authors contributed equally to this work.

Correspondence to: Prof. Nir Peled, MD, PhD, FCCP. Head of Helmsley Cancer Center, Shaare Zedek Medical Center, 12, Shmuel Beit St, Jerusalem, Israel. Email: nirp@szmc.org.il; Dr. Ariel Sobarzo, DVM, PhD, DICLAM. The Preclinical Research Center, Faculty of Health Sciences, Ben Gurion University of the Negev, Ben Gurion Avenue 4, Beer Sheva, 8410501, Israel; The Shraga Segal Department of Microbiology, Immunology, and Genetics, Faculty of Health Sciences, Ben-Gurion University of the Negev, Ben Gurion Avenue 4, Beer Sheva, Israel. Email: sobarzo@bgu.ac.il.

Background: Peripheral blood mononuclear cell (PBMC) humanized mouse models are essential for researching non-small cell lung cancer (NSCLC) treatments. However, these models are prone to xeno-graft versus host disease (xeno-GVHD), hampering their utility and requiring further investigation. This study examined xeno-GVHD responses from PBMCs of advanced-stage NSCLC patients compared to healthy donors (HDs) in a humanized peripheral blood lymphocyte (hu-PBL) model.

Methods: PBMCs from NSCLC patients and HDs were injected into immunocompromised NSG-SGM3 mice and monitored for eight weeks. xeno-GVHD progression was assessed through clinical examinations and flow cytometry of human T-cell levels in various tissues.

Results: Mice injected with PBMCs from HDs showed xeno-GVHD signs as early as 28 days post-injection, whereas those from NSCLC patients exhibited minimal signs, with only one model showing delayed responses by day 42. Clinical symptoms in mice included weight loss, anemia, low platelet counts, fur changes, and behavioral modifications. Flow cytometry of human PBMCs in mice indicated dominant $CD8^+$ effector memory T cells in peripheral blood. In contrast, $CD4^+$ effector memory T cells were predominant in the organs, with overall T cell levels lower in NSCLC models.

Conclusions: This study demonstrates significant differences in xeno-GVHD progression between advance-stage NSCLC patients and HDs, likely influenced by the patient's treatment histories. These findings improve our understanding of hu-PBL models for NSCLC research and may inform future treatment studies and strategies.

Keywords: Xeno-graft versus host disease (xeno-GVHD); non-small cell lung cancer (NSCLC); peripheral blood mononuclear cells (PBMCs); humanized mice; humanized peripheral blood lymphocyte model (hu-PBL model)

Submitted Sep 01, 2024. Accepted for publication Dec 24, 2024. Published online Apr 27, 2025.
doi: 10.21037/tlcr-24-787
View this article at: https://dx.doi.org/10.21037/tlcr-24-787

Introduction

Lung cancer (LC) is the most common cause of cancer-related mortality worldwide (1). Up to 85% of LC cases are non-small cell lung cancer (NSCLC), which often presents an advanced course of disease related to poor survival rates (2). Immunotherapy has revolutionized LC treatment and prolonged patient survival. However, the benefits of immunotherapies remain limited because most patients are unresponsive or relapse (3). Therefore, new treatment targets, therapeutics, and drug combinations are continuously being developed. Preclinical models that can replicate complex human tumor microenvironments and the interplay between tumor and immune cells are needed to improve our understanding and identify new therapeutics. Humanized mice, encompassing human immune cells engrafted on immunodeficient mice, have emerged in oncology, specifically LC, as a fundamental tool for drug discovery (4,5). The engraftment of human immune system components into immunodeficient mice can be achieved via several strategies with varying benefits and limitations. The humanized mouse model involves transplanting human-derived peripheral blood mononuclear cells (PBMCs) or hematopoietic stem cells (HSCs) into immunodeficient mice, thereby creating the humanized peripheral blood lymphocyte (hu-PBL) and the stem cell reconstituted (hu-SRC) models, respectively (3). The development of immunodeficient strains drove the emergence of humanized mouse models. These mice strains lack host adaptive immunity due to defective recombination of genes that encode antibodies and T cell receptors and reduce host innate immunity (4). As such, these models enable the development of human-like immune systems and the replication of a more "human microenvironment" for investigating tumor behavior analogous to that observed in cancer patients (6-8). Consequently, the integration of cell-line-derived xenografts (CDX) and patient-derived xenografts (PDX) within humanized mouse models represents a significant advancement, greatly enhancing the versatility of these models for investigating cancer pathogenesis and assessing therapeutic efficacy (8-10).

The hu-PBL model is the simplest and quickest of the two humanized models. Its ease of construction and rapid rate of humanization provide clear advantages over the hu-SRC model. It is widely used in immune-oncology research due to its accessibility, cost-effectiveness, ease of establishment (11,12) and ability to recapitulate higher levels of mature human T cells compared to the HSC model, including acquiring $CD3^+$ (5,7). However, a significant limitation of the hu-PBL model is the emergence of severe xeno-graft versus host disease (xeno-GVHD) primarily driven by activated human $CD4^+$ or $CD8^+$ T cells, which respond to mouse major histocompatibility (MHC) molecules (5,12-15). As a result, experimental timeframes are often curtailed and typically span only a few weeks, which is insufficient for evaluating treatment responses and immune reactions (7,12,14). Various strategies have been proposed to address this limitation by extending the experimental window until the onset of

Highlight box

Key findings

- We demonstrate that the onset and progression of xeno-graft versus host disease (xeno-GVHD) differ significantly between advanced-stage non-small cell lung cancer (NSCLC) patients and healthy donor-derived peripheral blood mononuclear cells (PBMCs) in the NSG-SGM3 mouse model. These findings are crucial for understanding the complex interactions between patient-specific factors and the development of xeno-GVHD. This knowledge is essential for designing and interpreting preclinical studies, particularly advanced-stage NSCLC. Furthermore, our study enhances the understanding of the functionality of immune cells in NSCLC patients, considering their treatment histories and clinical backgrounds.

What is known, and what is new?

- Humanized peripheral blood lymphocyte (hu-PBL) models are valuable tools for investigating new treatment strategies for patients with advanced-stage NSCLC. However, the development of xeno-GVHD, which significantly impacts these models, is not entirely understood.
- This study offers insights into the xeno-GVHD responses, showing that the functional state of T cells from advanced-stage NSCLC patients leads to a hampered progression and distinct phenotype of xeno-GVHD in the NSG-SGM3 hu-PBL model. We identify various T cell subpopulations in peripheral blood and organs, noting their differing levels among patients compared to healthy controls. Additionally, we highlight specific clinical factors in patients that may influence the development of xeno-GVHD.

What is the implication, and what should change now?

- The findings suggest that the functional states of PBMCs, influenced by patients' clinical backgrounds and treatment histories, should be carefully considered in preclinical models. This consideration can help better replicate patient-specific immune responses. Consequently, it may lead to more accurate evaluations of therapies for NSCLC in hu-PBL models. Ultimately, this approach could contribute to developing more effective personalized treatment strategies, especially for patients with advanced-stage NSCLC.

xeno-GVHD. These strategies include pre-depleting $CD4^+$ T cells or, more commonly, using MHC knockout mice such as NOG-dKO or NOG-β2 m, IAβdKO mice (11,16-18) In this respect, a novel triple transgenic NSG-SGM3 immunodeficient mouse strain has recently emerged. This strain of mice supported a diverse range of human immune cells, making them a key platform for studying interactions within the human immune system and tumor microenvironment (19). Additionally, PBMC pre-screening can de-risk donor selection for xeno-GVHD in the hu-PBL model to allow for more accurate testing of candidate drug efficacy (3).

Previous works have examined the impact of PBMCs from diverse patient groups on the onset and pathogenesis of xeno-GVHD (19-21). However, the influence of clinical factors on susceptibility to xeno-GVHD and the underlying pathogenic mechanisms induced specifically by PBMCs from advanced-stage NSCLC patients remains unknown. Here, we study clinical and cellular aspects of xeno-GVHD induced by advanced-stage NSCLC patient PBMCs versus those from healthy donors (HDs) in NSG-SGM3 mice to provide vital knowledge that could significantly advance the development of improved NSCLC hu-PBL models and pinpoint crucial insights into the functionality of the immune cells of NSCLC patients, considering their treatment histories and clinical backgrounds. We present this article in accordance with the ARRIVE reporting checklist (available at https://tlcr.amegroups.com/article/view/10.21037/tlcr-24-787/rc).

Methods

Mice

NSG-SGM3 mice expressing human *IL3*, *GM-CSF* (*CSF2*), and *SCF* (*KITLG*) were obtained from the Jackson Laboratory (Sacramento, CA, USA). Mice were maintained under specific pathogen-free conditions at Ben-Gurion University's animal facility. Experiments were performed under a project license (No. IL-59-11-2018) granted by the Institutional Animal Care and Use Committee of Ben Gurion University (BGU), in compliance with Israel Ministry of Health (MOH) national or institutional guidelines for the care and use of animals. All methods are reported according to the guidelines for reporting animal experiments.

Isolation of PBMCs

PBMCs from advanced-stage NSCLC patients and HDs were collected from peripheral blood samples following an informed consent form (ICF) signing at Soroka University Medical Center. The sample size analyzed during this study reflected the number of eligible patient donors available to us. Control samples were collected to match the patients' sample size group. Approximately 50–100 mL of peripheral whole blood was collected via standard venipuncture techniques into 10-mL phlebotomy tubes, anticoagulated with ethylenediaminetetraacetic acid (EDTA) or Sodium Citrate. PBMCs were isolated immediately after phlebotomy using the commercialized kit (SepMate or CPT tubes) according to the manufacturer's instructions (Stemcell and BD Medical Technologies, respectively). Following isolation, PBMCs were aliquoted and transplanted freshly to NSG-SGM3 mice. The study was conducted in accordance with the Declaration of Helsinki (as revised in 2013). The ethics committee of Soroka Medical Center (No. 0026-19-SOR) approved the study. Informed consent was obtained from all subjects and their legal guardians.

Creation of hu-PBL mice and assessment of xeno-GVHD response

Blood samples were drawn from advanced-stage NSCLC patients (n=4) and HDs (n=4), and PBMCs were isolated and intravenously injected into 2/3 female NSG-SGM3 mice per patient/donor. An additional control group of mice was injected with physiologic saline (Ctrl) (n=2). After isolating human PBMCs, 5×10^6 PBMCs were randomly injected intravenously into the tail vein of NSG-SGM3 mice aged 10–12 weeks. Mice were monitored bi-weekly for the development of xeno-GVHD for a total period of eight weeks. Both clinical signs and cellular components were assessed. A schematic illustration of the study plan is presented in *Figure 1A*. A scoring system was used to evaluate the severity of xeno-GVHD based on previously reported work (20). We assessed the following mice parameters: weight loss, blood cell, fur and skin appearance, behavior changes, and pain signs (activity, posture, and fur loss). Each parameter received a rating between zero and two twice weekly (Table S1). Once a mouse reached the human endpoint criteria (presented >15% weight loss from starting weight, progressive anemia >20%, generalized

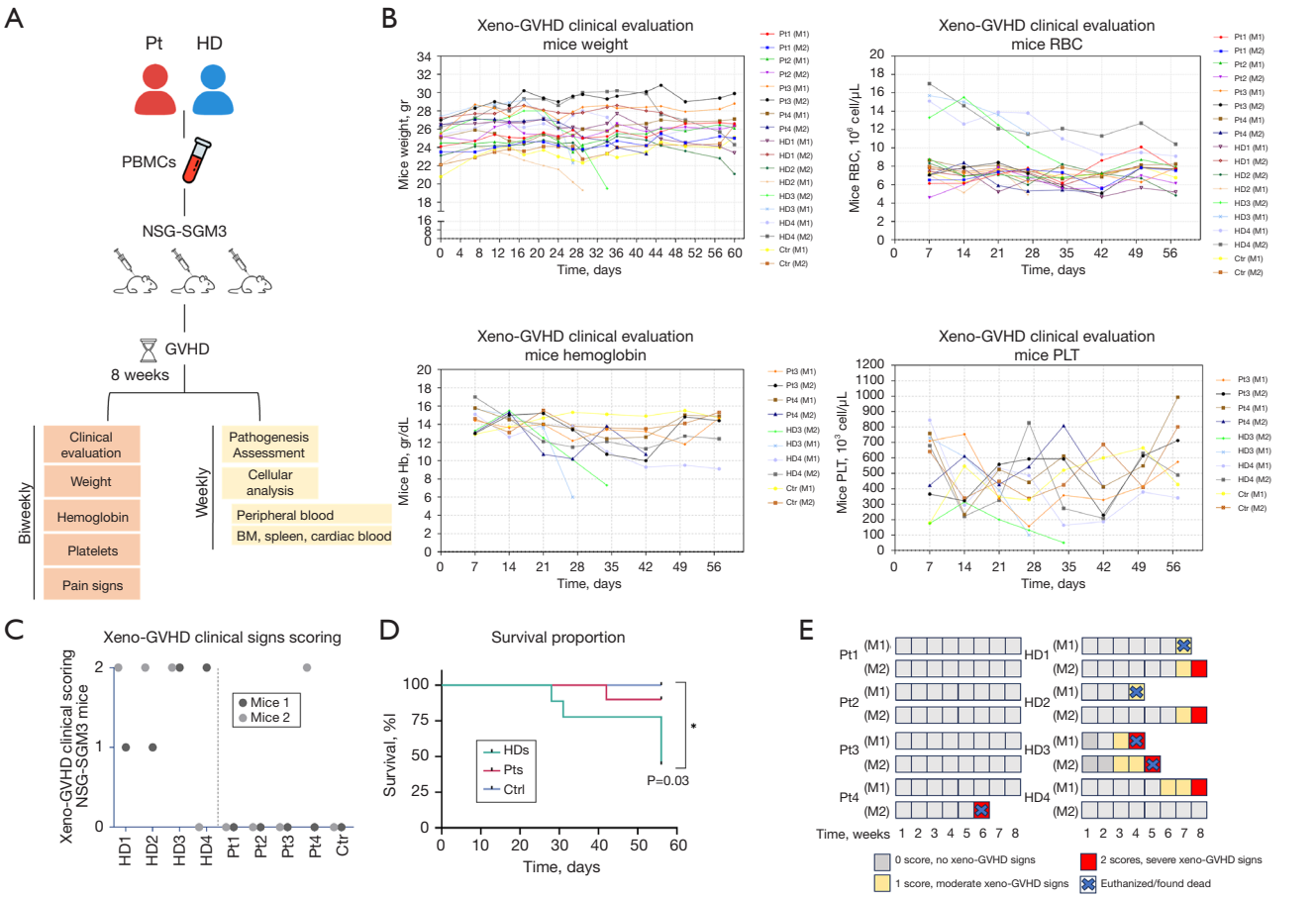

Figure 1 Study design and clinical evaluation of xeno-GVHD. (A) This schematic illustrates the study design. Blood samples were collected from NSCLC patients and HDs. PBMCs were isolated and intravenously injected into NSG-SGM3 mice (n=2 for each donor). Over eight weeks, the mice were monitored for xeno-GVHD development. (B) xeno-GVHD responses were evaluated by tracking weight, hemoglobin levels, red blood cells, and platelet counts of NSG-SGM3 hu-PBL (human peripheral blood lymphocytes) models of patients, HDs, and control groups (Ctrls), which received saline only. Monitoring was done over the eight weeks. Hemoglobin and platelet count measurements were absent for Pt 1 and 2 and HD 1 and 2. (C) The onset of clinical signs of xeno-GVHD in mice injected with PBMCs from patients, HDs, and Ctrls were recorded. A scoring system was used: 0 = no signs of xeno-GVHD, 1 = moderate signs, 2 = severe signs. The severity of xeno-GVHD was assessed based on weight loss percentage, anemia, clinical appearance, and behavior of the NSG-SGM3 mice that received PBMCs. (D) Survival curves of NSG-SGM3 mice injected with PBMCs from patients, HDs, and Ctrls groups are presented. Statistical significance was determined using the log-rank test with: *, P value <0.05. (E) This schematic illustrates the time point of detecting xeno-GVHD appearance, response, and mice outcome of hu-PBL models from patients and HDs. The xeno-GVHD score is described in Table S1. The color code indicates gray, with a 0 score of no signs of xeno-GVHD, a yellow score of 1, moderate response, and a red score of 2, severe xeno-GVHD response. Blue X indicates the mice's death. BM, bone marrow; Hb, hemoglobin; HDs, healthy donors; M, mice; NSCLC, non-small cell lung cancer; Pts, patients; PLT, platelet; PBMCs, peripheral blood mononuclear cells; RBC, red blood cells; xeno-GVHD, xeno-graft versus host disease.

fur loss (>25%), inflamed skin or obvious pain signs (expressed by animal posture, mobility, and appearance), it was sacrificed. Peripheral blood was sampled from each mouse every week for Flow cytometry analysis. Cord blood (CB), bone marrow (BM) cells, and spleen stroma were also collected and analyzed from euthanized mice. Sampling ordering and collection time were constantly done to minimize potential confounders. Two independent members

of the lab performed experiments and data analysis. No animals were excluded from our study.

Preparation of CB, BM, and spleen samples for flow cytometry analysis

Mice displaying apparent signs and symptoms of xeno-GVHD were euthanized, and CB was drawn directly from the heart into tubes anticoagulated with either EDTA or sodium citrate. Spleens were dissected from the abdominal cavity, and the harvested tissue was minced through a sterile dish before being gently passed through a mesh strainer. The tissue and cells were washed using PBS, centrifuged, and washed again. For BM cell preparation, femoral and pelvic bones were dissected, and all remaining bone tissue was removed. Each bone end was excised, and BM was expelled. CB, BM, and spleen cells were transferred for flow cytometry analysis following preparation.

Antibody staining and flow cytometry

Peripheral blood (volume of 100 µL) was withdrawn from hu-PBL NSG-SGM3 mice every week and was processed for flow cytometry. Briefly, erythrocytes were depleted using an RBC lysis solution (Milteny Biotec). Cells were then washed with PBS FACS buffer (PBS pH 7.2, 0.5% BSA, 2 mM EDTA) and resuspended in the desired surface stains. Following 10 min incubation in 4 ℃, flow cytometry data acquisition was performed using BD FACS ARIATM III, and analysis was done using FlowJo software (Tree Star). A T-cell panel characterizing the T-cell subpopulation and activation state was designed to assess human immune cell presence in the HuPBMC NSG-SGM3 mice and investigate the process of xeno-GVHD. Antibodies used for human PBMC characterization included anti-human CD45, CD3, CD4, and CD8. For T cell phenotype, we used anti-human: CD45RA and CD197 (Milteny Biotec). Live or dead cells were detected using Ghost Dye RedTM 710 (TONBO biosciences). Anti-mouse CD45 antibodies were used to detect mouse immune cells and discriminate between mouse and human cells.

Statistical analysis

Statistical analyses were performed using GraphPad Prism 8.4.2. A two-tailed unpaired *t*-test was employed to determine the statistical significance between NSCLC patients and HD groups, with a P value of <0.05 considered statistically significant. Assumptions of normality, equal variances, and proportional hazards were checked using appropriate tests, and data transformations were applied if needed.

Results

Clinical characteristics of NSCLC patients

To examine the potential effect of NSCLC patients clinical factors on the development and severity of xeno-GvHD response in mice, the following clinical characteristics of NSCLC patients were obtained: histopathological diagnosis, disease stage, DNA alterations, and treatment history. Data presented in *Table 1* showed that two NSCLC patients had adenocarcinoma (Pt1 and Pt4), and two (Pt2 and Pt3) had squamous cell carcinoma. All patients had an advanced disease (stage IV) and were previously treated with chemotherapy and immunotherapy. Specific mutations detected in NSCLC patients included KRAS in Pt1 and Pt2, *BRAF* in Pt3, and *ALK* in Pt4.

Clinical evaluation of xeno-GVHD in NSG-SGM3 mice

The progression of xeno-GVHD responses in the hu-PBL model was evaluated by mice's clinical presentation, which was examined twice a week. This comprised weight tracking, behavior monitoring, hematological changes, and pain signs associated with xeno-GVHD.

The results presented in *Figure 1B* demonstrate that mice injected with PBMCs from HDs compared to patients exhibited more profound and earlier xeno-GVHD responses. These included weight loss with a rapid decline of RBC, hemoglobin, and platelet counts. The earliest signs of severe xeno-GVHD were documented on day 28 post-injection of PBMCs for HDs and on day 42 after the injection of patients. Correspondingly, visible pain signs were more profound in HD mice (*Figure 1C*). Survival analysis revealed a significant difference (P=0.03) in the outcomes between mice injected with PBMCs from HDs and those injected with PBMCs from patients (*Figure 1D*). HD mice exhibited a significantly lower median survival time (56 days). The median survival time in the patients group was comparable to that of the Ctrl group, with both groups surviving until the experiment's endpoint (*Figure 1D*). Overall, mice from all four HD models exhibited xeno-GVHD responses, with half not surviving the duration of

Table 1 Clinical characteristics of selected NSCLC patients whose PBMCs were used for creation of hu-PBL mice

Patients	Age (years)	Diagnosis	Stage	Genetic alterations	Treatment history	Treatment during PBMC sampling
Pt1	63	NSCLC adenocarcinoma	IV	FMI KRAS G12A STK11 E33fs*14 TP53 R248L	12.2016: cisplatin/pemetrexed/ bevacizumab X5 with significant PR 3.2017: Alimta + Keytruda with metabolic CR (stop Alimta at 9.2017 and continue Keytruda)	Keytruda single agent
Pt2	48	Squamous NSCLC	IV	KRAS G12C/STK11 deletion exon 1/Myc amp/CDC73/CDKN2A/ B/RAD21 amp/TP53 R196	3.2019: carboplatin/taxol/Keytruda 5.2019: Keytruda/carboplatin/Gemzar 7.2019: nivolumab/ipilimumab/imiquimode 10.2019: anakinra/nivolumab 2.2019: Navelbine	Navelbine
Pt3	64	Squamous NSCLC	IV	BRAF G469V 9.8%; ARID1A 15%; TP53 12%	12.2019: carboplatin/Taxol/Keytruda X5 and palliative radiation with metabolic near CR 3.2020: Keytruda single agent continue X6 7.2020: continue Keytuda/Navelbine	Keytruda single agent
Pt4	71	NSCLC adenocarcinoma	IV	ALK, EGFR negative	11.2017: cisplatin/Alimta Since 12.2017: nivolumab 4.2018: palliative XRT to LUL	Nivolumab cycle 48/51

CR, complete response; hu-PBL, human peripheral blood lymphocytes; LUL, left upper lung; NSCLC, non-small cell lung cancer; PBMCs, peripheral blood mononuclear cells; PR, partial response; XRT, radiation therapy.

the experiment. In contrast, only one patient (Pt4) triggered a xeno-GVHD reaction in mice, while the other patient models did not produce any visible clinical response (*Figure 1E*).

Cellular evaluation of human T-cell composition in hu-PBL mice model

In addition to evaluating the mice clinically, we monitored the progression of xeno-GVHD development in our hu-PBL model through T-cell flow cytometry analysis of the injected human PBMCs. This allowed us to identify specific cellular components associated with early and late xeno-GVHD responses. Analyses were conducted at four different time points, representing different xeno-GVHD stages: baseline (0 weeks), early (4 weeks), intermediate (6 weeks), and late (8 weeks). The flow cytometry gating strategy is illustrated in Figure S1.

T-cells baseline levels of hu-PBL models

The baseline results presented in *Figure 2* indicated that the levels of $CD45^+$ and $CD3^+$ cells were significantly higher in the HD group (*Figure 2A*). In contrast, there were only minor variations in the percentages of $CD4^+$ and $CD8^+$ T cells between patients and HDs. Specifically, the proportion of $CD4^+$ T cells was 54.98% for HDs and 61.13% for patients, while $CD8^+$ T cells were 36.3% for HDs and 33.5% for patients (*Figure 2B*).

Analysis of T-cell subpopulations revealed notable differences between the two groups. There were statistically significantly higher levels of central memory (CM) $CD8^+$ T cells in NSCLC patients (P=0.03), whereas naïve $CD4^+$ and $CD8^+$ T cell levels were more elevated in HDs (*Figure 2C,2D*). The complete percentage distribution of T-cells in patients and HDs is shown in *Figure 2E*.

Human T cell levels in hu-PBL models: four weeks post-injection

We examined the T-cell composition in our hu-PBL model four weeks after injection to identify the cellular responses associated with the clinical changes xeno-GVHD observed in mice. Our findings revealed a statistically significant difference in T-cell counts; $CD45^+$ and $CD3^+$ cells were

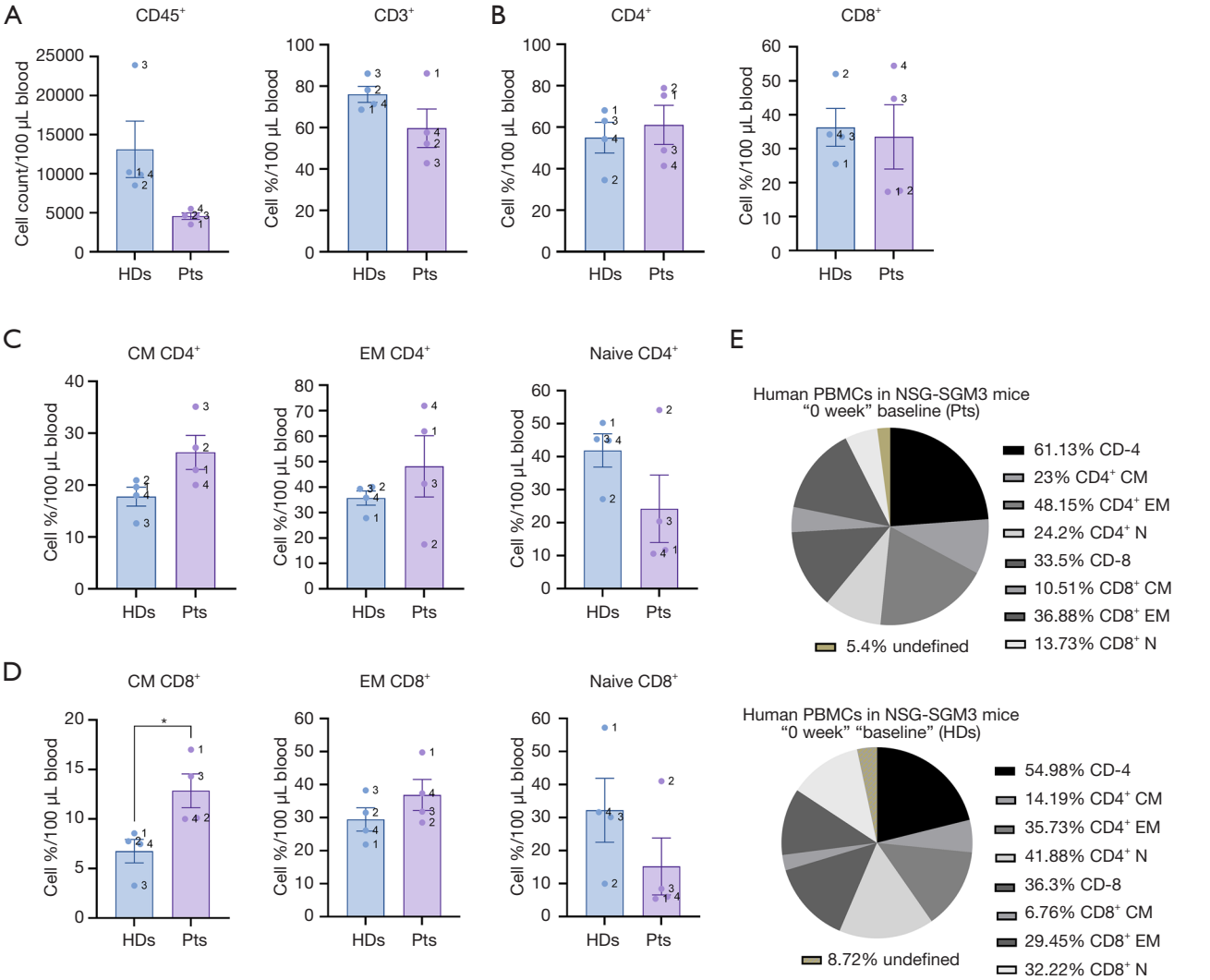

Figure 2 Baseline T-cell analysis of PBMCs injected into hu-PBL mice model. PBMCs were collected from NSCLC patients (n=4) and HDs (n=4). These cells were then intravenously injected into NSG-SGM3 mice (n=2 for each donor) to create hu-PBL models. Flow cytometry baseline results for T-cell compartments and subpopulations at point 0 are presented for both patients and HDs. Human and mouse PBMCs were distinguished using specific CD45$^+$ antibodies. Following this, CD3$^+$ cells were analyzed for their CD4$^+$ and CD8$^+$populations and subpopulations, including CM, EM, and naïve cells. (A) CD45$^+$ and CD3$^+$ cell populations. (B) CD4$^+$ and CD8$^+$ T cells. (C) CD4$^+$ T cell subpopulations (CM, EM, and naïve). (D) CD8$^+$ T cells subpopulations (CM, EM, and naïve). The bar charts display the mean results with SEM for HDs (light blue) and patients (light purple). Individual patients and HDs are identified by numbers 1–4. A two-tailed unpaired *t*-test was used to determine statistical significance between groups, with a P value of <0.05 considered statistically significant. The following notations indicate levels of significance: *, P<0.05. (E) Pie charts illustrating the mean frequencies of CD4$^+$ and CD8$^+$ positive T cells and their subpopulations in patients (upper panel) and HDs (lower panel). T-cell results are expressed as percentages of CD3$^+$ cells. T cell subpopulations are expressed as percentages of CD4$^+$ and CD8$^+$ cells. CM, central memory; EM, effector memory; hu-PBL, human peripheral blood lymphocytes; HDs, healthy donors; NSCLC, non-small cell lung cancer; Pts, patients; PBMCs, peripheral blood mononuclear cells; SEM, standard error of the mean.

found in higher numbers in HDs than patients, with P values of 0.008 and 0.0001, respectively (*Figure 3A*). The levels of $CD4^+$ T cells were similar between the two groups. However, the levels of $CD8^+$ T cells were nearly doubled in HDs, at 67.51%, compared to 35.08% in patients (*Figure 3B*). Interestingly, the ratio of $CD4^+/CD8^+$ T cells was higher in patients, yielding values of 42.06%/35.08% in patients compared to 30.05%/67.51% in HDs (*Figure 3B*).

Further analysis of T-cell subpopulations revealed that the dominant subtype in both groups was effector memory (EM) T cells. However, HDs displayed significantly higher percentages: 89.3% of $CD4^+$ T cells and 87.1% of $CD8^+$ T cells, compared to 44% of $CD4^+$ T cells and 48% of $CD8^+$ T cells in patients (*Figure 3C,3D*). A statistically significant difference was noted in the EM $CD4^+$ T cells between HDs and patients, with a P value of 0.009 (*Figure 3C*).

Naïve T cells constituted the most minor proportion, accounting for less than 1% of the $CD4^+$ and $CD8^+$ T cell groups. A significant difference was observed in the CM $CD4^+$ T cells between HDs and patients, with 9.05% in HDs and 0% in patients (P=0.02, *Figure 3C*). The complete distribution of T cells in patients and HDs four weeks post-injection is shown in *Figure 3E*.

Human T cell levels in the hu-PBL model: six weeks post-injection

Analysis of T-cell composition in the hu-PBL models six weeks after injection showed results consistent with those observed four weeks post-injection, indicating a growing discrepancy between HDs and patients groups. HDs exhibited an average count of 663.4 $CD45^+$ cells, significantly higher than 40.58 in patients, with a statistical significance of P=0.02. The rate of $CD3^+$ T cells was also notably higher in HDs, approximately double that of patients (98% *vs.* 60%) (*Figure 4A*). Furthermore, the percentage of $CD8^+$ T cells in HDs was four times greater at 62.34%, compared to 11.02% in patients, which was statistically significant with a P value of 0.001. Conversely, the proportion of $CD4^+$ T cells was higher in the patients group, reaching 56.01%, while HDs had 36.71% (*Figure 4B*). Additionally, the $CD4^+/CD8^+$ T cell ratio differed significantly between the groups: 62%/10% for patients and 36.23%/62.86% for HDs (*Figure 4B*).

T-cell subpopulation analysis revealed that EM $CD4^+$ and $CD8^+$ T cells were the predominant subtypes, whereas the percentage of naïve T cells was low (*Figure 4C,4D*). HDs showed higher EM $CD8^+$ T cells than patients (96.95% *vs.* 48.43%). *Figure 4E* illustrates the complete distribution of T cells in patients and HDs six weeks post-injection. Figure S2 provides an example of the raw data results from flow cytometry at week 6 following the PBMC injection.

Human T cell levels in hu-PBL models: eight weeks post-injection

An analysis of T-cell composition in the hu-PBL models in the progressed stage of xeno-GVHD response eight weeks post-injection revealed a similar pattern for both groups. However, a noticeable decrease in T-cell count and percentage was observed in both populations. The count of $CD45^+$ cells was significantly reduced in both groups, with HDs showing a considerably higher average cell count of 79 compared to 15 in patients, with a statistically significant P value of 0.02 (see *Figure 5A*).

The rate of $CD8^+$ T cells was significantly higher in HDs at 48.23%, while only 11.06% in patients (P value of 0.04). Conversely, the percentage of $CD4^+$ T cells was slightly more significant in patients, with a rate of 63.3% compared to 50.27% in HDs (*Figure 5B*). The $CD4^+/CD8^+$ T cell ratios were 50.27%/48.23% for HDs and 63%/11% for patients. T-cell subpopulations demonstrated variable differences, with a predominant presence of EM T cells and no naïve T cells detected (*Figure 5C,5D*). The complete distribution of T cells in patients and HDs eight weeks post-injection is illustrated in *Figure 5E*.

Kinetic analysis of human T-cell levels in hu-PBL models

We compared the T-cell composition between the different time points (0, 4, 6, and 8 weeks) to assess cellular levels over time and identify the kinetic profiles of various T-cell compartments in our hu-PBL models. We found that HDs exhibited a statistically significant decrease in $CD45^+$ cell count, with a P value of 0.0001 when comparing baseline measurements to all subsequent time points (see *Figure 6A*). The percentage levels of $CD4^+$ and $CD8^+$ T-cells showed moderate fluctuations. There was a decrease in $CD4^+$ levels between baseline and 4 weeks post-injection, alongside an increase in $CD8^+$ levels during the same period (see *Figure 6B*).

We observed significant changes in $CD4^+$ subpopulations, specifically a decrease in CM T-cells when comparing 0 to 8 weeks (P=0.02) and a decrease in naïve T-cells from baseline to all-time points (P value of <0.001). In contrast, there was an increase in EM T-cells from baseline to all-time points (0–4, P value of 0.04, 0–6, P value of 0.005, 0–8, P value of

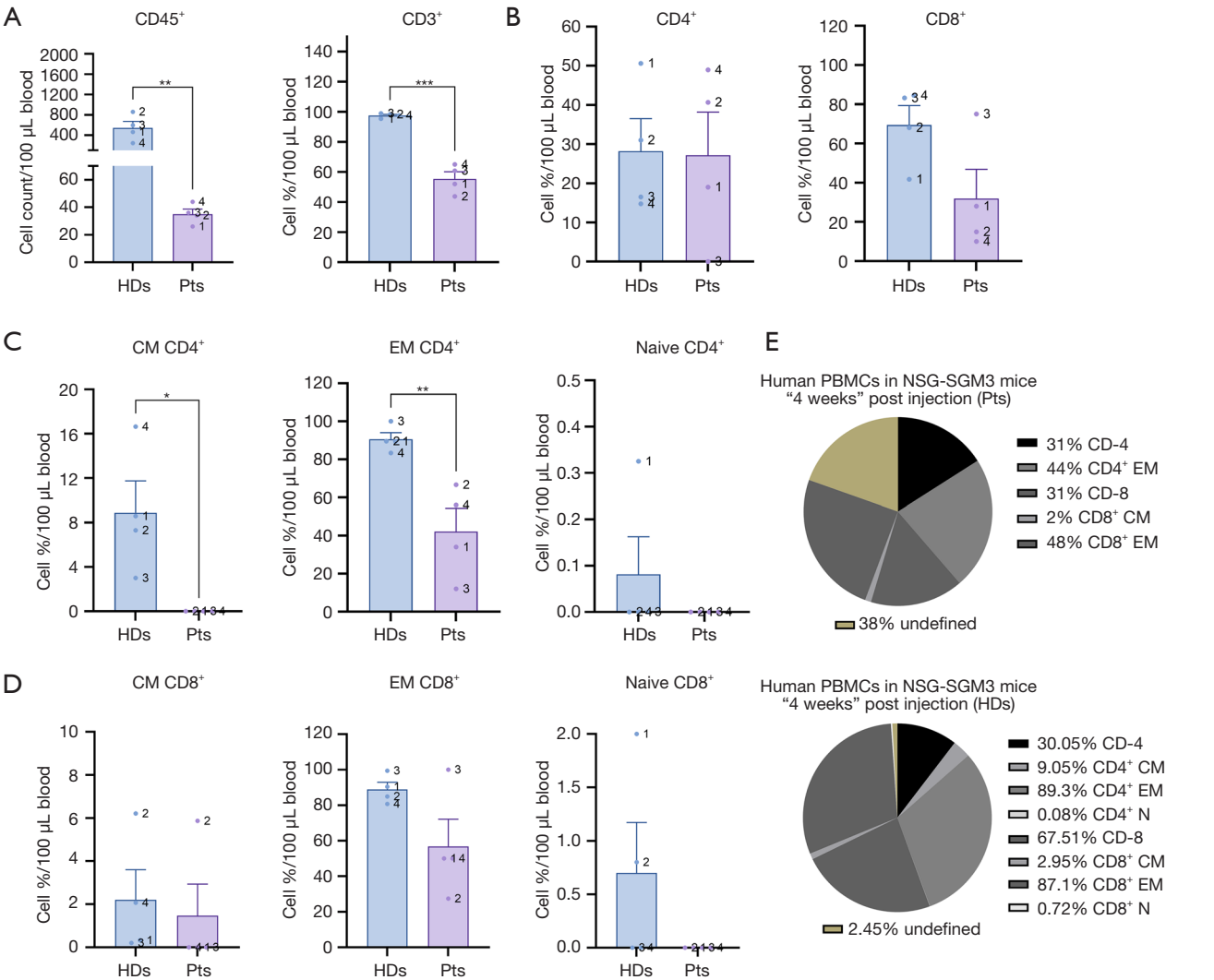

Figure 3 T-cell analysis of PBMCs from hu-PBL mice model 4 weeks post-injection. PBMCs were collected from NSCLC patients (n=4) and HDs (n=4). These cells were then intravenously injected into NSG-SGM3 mice (n=2 for each donor) to create hu-PBL models. Flow cytometry baseline results for T-cell compartments and subpopulations 4 weeks post-injection are presented for both patients and HDs. Human and mouse PBMCs were distinguished using specific CD45$^+$ antibodies. Following this, CD3$^+$ cells were analyzed for their CD4$^+$ and CD8$^+$ populations and subpopulations, including CM, EM, and naïve cells. (A) CD45$^+$ and CD3$^+$ cell populations. (B) CD4$^+$ and CD8$^+$ T cells. (C) CD4$^+$ T cell subpopulations (CM, EM, and naïve). (D) CD8$^+$ T cells subpopulations (CM, EM, and naïve). The bar charts display the mean results with SEM for HDs (light blue) and patients (light purple). Individual patients and HDs are identified by numbers 1–4. A two-tailed unpaired *t*-test was used to determine statistical significance between groups, with a P value of <0.05 considered statistically significant. The following notations indicate levels of significance: *, P<0.05; **, P<0.01; ***, P<0.001. (E) Pie charts illustrating the mean frequencies of CD4$^+$ and CD8$^+$ positive T cells and their subpopulations in patients (upper panel) and HDs (lower panel). T-cell results are expressed as percentages of CD3$^+$ cells. T cell subpopulations are expressed as percentages of CD4$^+$ and CD8$^+$ cells. CM, central memory; EM, effector memory; PBMCs, peripheral blood mononuclear cells; hu-PBL, human peripheral blood lymphocytes; HDs, healthy donors; NSCLC, non-small cell lung cancer; Pts, patients; SEM, standard error of the mean.

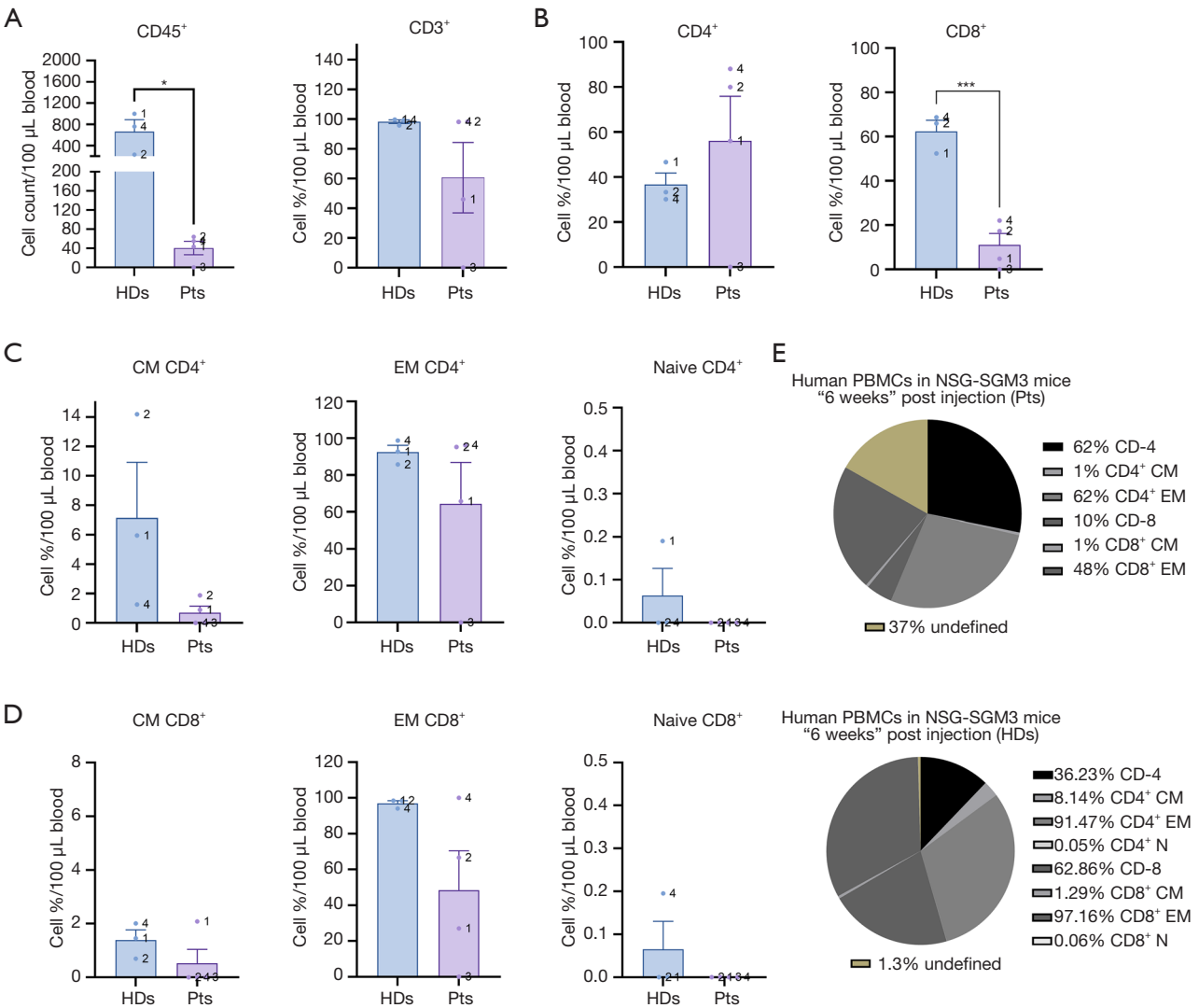

Figure 4 T-cell analysis of PBMCs from hu-PBL mice model 6 weeks post-injection. PBMCs were collected from NSCLC patients (n=4) and HDs (n=4). These cells were then intravenously injected into NSG-SGM3 mice (n=2 for each donor) to create hu-PBL models. Flow cytometry baseline results for T-cell compartments and subpopulations 6 weeks post-injection are presented for both patients and HDs. Human and mouse PBMCs were distinguished using specific CD45$^+$ antibodies. Following this, CD3$^+$ cells were analyzed for their CD4$^+$ and CD8$^+$ populations and subpopulations, including CM, EM, and naïve cells. (A) CD45$^+$ and CD3$^+$ cell populations. (B) CD4$^+$ and CD8$^+$ T cells. (C) CD4$^+$ T cell subpopulations (CM, EM, and naïve). (D) CD8$^+$ T cells subpopulations (CM, EM, and naïve). The bar charts display the mean results with SEM for HDs (light blue) and patients (light purple). Individual patients and HDs are identified by numbers 1–4. A two-tailed unpaired *t*-test was used to determine statistical significance between groups, with a P value of <0.05 considered statistically significant. The following notations indicate levels of significance: *, P<0.05; ***, P<0.001. (E) Pie charts illustrating the mean frequencies of CD4$^+$ and CD8$^+$ positive T cells and their subpopulations in patients (upper panel) and HDs (lower panel). T-cell results are expressed as percentages of CD3$^+$ cells. T cell subpopulations are expressed as percentages of CD4$^+$ and CD8$^+$ cells. CM, central memory; EM, effector memory; hu-PBL, human peripheral blood lymphocytes; HDs, healthy donors; NSCLC, non-small cell lung cancer; Pts, patients; PBMCs, peripheral blood mononuclear cells; SEM, standard error of the mean.

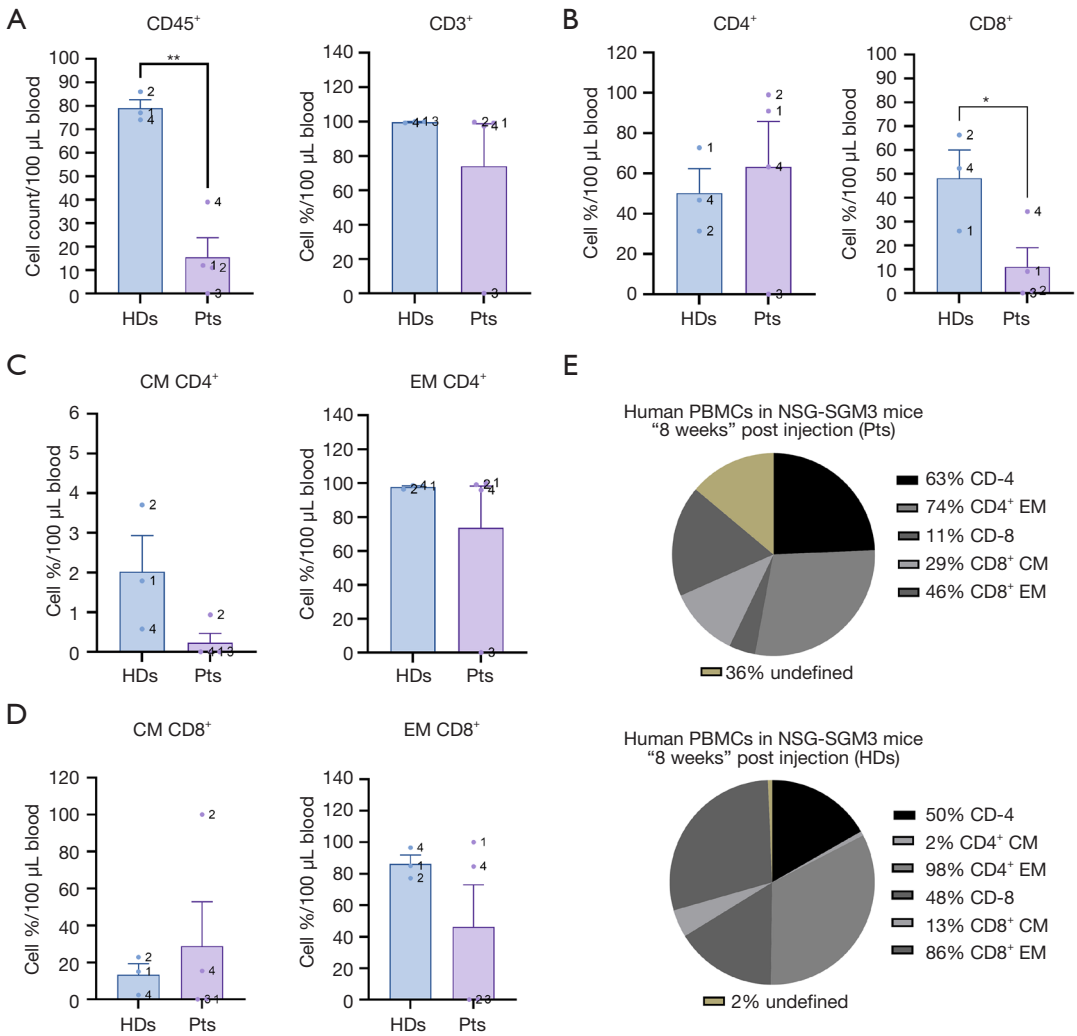

Figure 5 T-cell analysis of PBMCs from hu-PBL mice model 8 weeks post-injection. PBMCs were collected from NSCLC patients (n=4) and HDs (n=4). These cells were then intravenously injected into NSG-SGM3 mice (n=2 for each donor) to create hu-PBL models. Flow cytometry baseline results for T-cell compartments and subpopulations 8 weeks post-injection are presented for both patients and HDs. Human and mouse PBMCs were distinguished using specific $CD45^+$ antibodies. Following this, $CD3^+$ cells were analyzed for their $CD4^+$ and $CD8^+$ populations and subpopulations, including CM, EM, and naïve cells. (A) $CD45^+$ and $CD3^+$ cell populations. (B) $CD4^+$ and $CD8^+$ T cells. (C) $CD4^+$ T cell subpopulations (CM, EM, and naïve). (D) $CD8^+$ T cells subpopulations (CM, EM, and naïve). The bar charts display the mean results with SEM for HDs (light blue) and patients (light purple). Individual patients and HDs are identified by numbers 1–4. A two-tailed unpaired *t*-test was used to determine statistical significance between groups, with a P value of <0.05 considered statistically significant. The following notations indicate levels of significance: *, P<0.05; **, P<0.01. (E) Pie charts illustrating the mean frequencies of $CD4^+$ and $CD8^+$ positive T cells and their subpopulations in patients (upper panel) and HDs (lower panel). T-cell results are expressed as percentages of $CD3^+$ cells. T cell subpopulations are expressed as percentages of $CD4^+$ and $CD8^+$ cells. CM, central memory; EM, effector memory; hu-PBL, human peripheral blood lymphocytes; HDs, healthy donors; NSCLC, non-small cell lung cancer; Pts, patients; PBMCs, peripheral blood mononuclear cells; SEM, standard error of the mean.

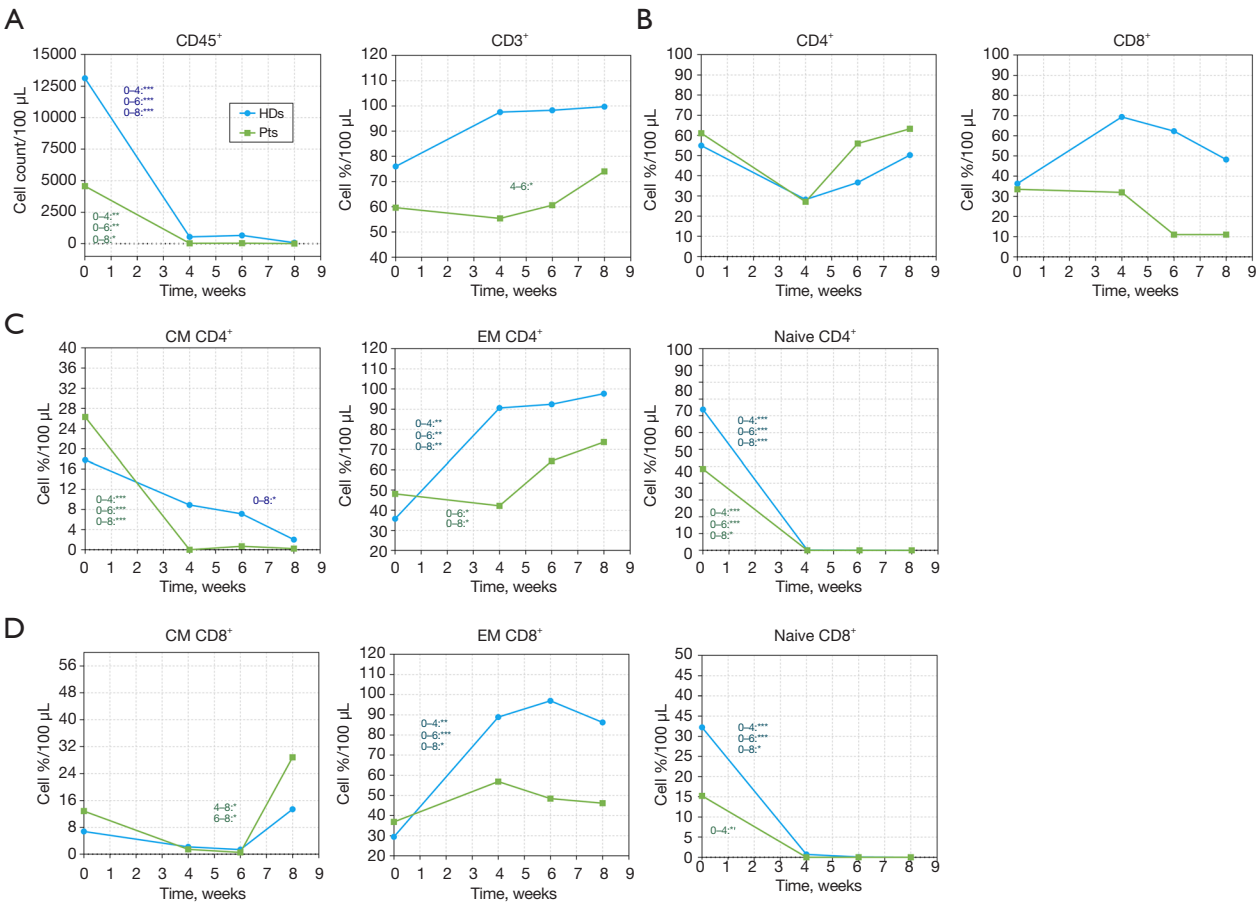

Figure 6 T-cell kinetics of NSCLC patients and healthy donors hu-PBL model. PBMCs were collected from NSCLC patients and HDs (n=4 for each group). These cells were injected into NSG-SGM3 mice, with two mice assigned to each donor, to establish hu-PBL models. Blood samples (100 µL) were collected from the tail veins of the hu-PBL model mice at three different time points: 4, 6, and 8 weeks post PBMC injection. An additional baseline sample (time point 0) was collected before the injection. Flow cytometry assessed the human T-cell compartments and subpopulations, allowing for comparative analyses across these time points. (A) $CD45^+$ cell count and percentage of $CD3^+$ T cells. (B) $CD4^+$ and $CD8^+$ T cells. (C) $CD4^+$ subtypes, including CM T cells, EM T cells, and naïve T cells. (D) $CD8^+$ T cells and their subtypes, including CM T cells, EM T cells, and naïve T cells. The mean values and P values for the comparisons are presented. A two-tailed ANOVA was performed to determine the statistical significance between time points for HDs and patients, with a significance level set at P<0.05. The following notations indicate the significance levels: *, P<0.05; **, P<0.01; ***, P<0.001. Color code: HDs, blue; Pts, green. ANOVA, analysis of variance; CM, central memory; EM, effector memory; hu-PBL, human peripheral blood lymphocytes; HDs, healthy donors; NSCLC, non-small cell lung cancer; Pts, patients; PBMCs, peripheral blood mononuclear cells.

0.008), as illustrated in *Figure 6C*. Significant changes were also observed in $CD8^+$ subpopulations, with an increase in EM T-cells and a decrease in naïve T-cells. The P values for these changes were 0.0018, 0.001, and 0.015 when comparing the baseline to 4, 6, and 8 weeks respectively.

Analysis in patients revealed compatible T-cell responses as HDs with additional T-cell subpopulations demonstrated significant changes. Statistically significant levels were detected for $CD45^+$ cell count (*Figure 6A*), all $CD4^+$ subpopulations (*Figure 6C*), and naïve $CD8^+$ T-cells (*Figure 6D*). Only in this group were additional significant changes observed, which included an increase in the percentage of $CD3^+$ T-cells when comparing 4 to 6 weeks (P=0.044) and an increase in CM $CD8^+$ T-cells (comparing 4 to 6 weeks, P=0.02, and 6 to 8 weeks, P=0.02). In contrast to HDs, no significant changes were detected in EM $CD8^+$

T-cells across the different time points.

Human T-cell levels in mice organs of hu-PBL models

To enhance our understanding of the progression of xeno-GVHD responses and their link to T-cell levels, we collected BM, spleen, and CB from hu-PBL NSG-SGM3 mice for T-cell analysis. We analyzed HDs and patients mice that exhibited severe clinical xeno-GVHD responses and those that did not. The cellular analysis was conducted as previously described above.

For severe xeno-GVHD, we examined two mice from the hu-PBL model: HD3 (M1, see *Figure 1E*), which showed the earliest signs of severe xeno-GVHD by week 4 post-injection, ultimately leading to the mouse's death, and Pt4 (M2, see *Figure 1E*), the only patient model that demonstrated signs of xeno-GVHD, which also resulted in the mouse's death at week 6 (see *Figure 7A-7D*).

The HD3 and Pt4 models had the highest number of $CD45^+$ cells in the spleen, followed by BM and CB. The percentage of $CD3^+$ T cells was highest in the CB, with HD3 showing a more significant proportion than Pt4 across all organs (*Figure 7A*). $CD4^+$ T cell levels were similar in all organs, but Pt4 had slightly higher levels. $CD8^+$ cells were most abundant in CB, and HD3 had twice as many $CD8^+$ cells as Pt4 in all organs (*Figure 7B*). For the $CD4^+$ subpopulation (*Figure 7C*), HD3 had the highest CM $CD4^+$ T cells in CB, while Pt4 had more in the BM. HD3's CB levels were six times higher than Pt4's. Naïve $CD4^+$ T cells were most prevalent in CB, with Pt4 exhibiting higher levels. In the $CD8^+$ analysis (*Figure 7D*), Pt4 had the highest CM $CD8^+$ T cells in the spleen, whereas HD3 only detected cells in CB. EM $CD8^+$ cells were similar in both models, but HD3 had higher levels than Pt4. Naïve $CD8^+$ cells were mainly in Pt4, with the highest levels in the spleen.

T-cell responses were also assessed in hu-PBL mouse models without xeno-GVHD, HD4 (M2), and Pt4 (M1) eight weeks post-injection. Consisting with the severe xeno-GVHD models, the highest $CD45^+$ cell counts were found in the spleen, followed by BM and CB, but these counts were roughly half of those seen in severe models. Similar $CD3^+$ cell rates were observed across HD4 and Pt4 models and organs (*Figure 7E*). While total $CD4^+$ cells were higher in Pt4 than in HD4, $CD8^+$ levels were significantly elevated in HD4 across all organs, with Pt4 showing minimal levels (*Figure 7F*). For $CD4^+$ subpopulations, CM and EM $CD4^+$ cells were similar in both models. Naïve $CD4^+$ cells were only present in Pt4, especially in the BM (*Figure 7G*). $CD8^+$ analysis revealed high CM $CD8^+$ levels in the spleen and naïve cells in Pt4's BM. HD4 exhibited similar EM $CD8^+$ cell levels across all organs, while Pt4 showed almost no EM $CD8^+$ cells in CB (*Figure 7H*).

A further examination of the two different Pt4 hu-PBL mouse models revealed significantly elevated levels in several T-cell compartments, particularly in mice with severe xeno-GVHD. Notably, the $CD45^+$ cell counts were twice as high across all organs, and $CD8^+$ cell counts were 20-fold more significant in all organs. Additionally, there were increased levels of naïve $CD4^+$ cells in the CB, CM $CD8^+$ T cells in the BM, EM $CD8^+$ T cells in the CB, and naïve $CD8^+$ T cells in the BM and CB. In contrast, Pt4 mice that did not exhibit clinical xeno-GVHD responses showed higher levels of CM $CD4^+$ T cells in all organs and an increased number of naïve $CD8^+$ T cells in the BM.

Discussion

The clinical significance of studying NSCLC in its advanced stages is critically important (21,22). Humanized mouse models serve as essential preclinical platforms for investigating advanced NSCLC, where the complexity of tumor-immune interactions is most prominent (4,6-8,12). However, a significant limitation of these models, particularly the hu-PBL variant, is the occurrence of xeno-GVHD, which can restrict their utility and is influenced by both the donor and the recipient (23,24). Additionally, research on xeno-GVHD responses has underscored the significance of multi-faceted immune cell interactions (24-26). There is still limited evidence regarding the role of T-cell subpopulations in this process, particularly in patients with advanced NSCLC. To enhance our understanding, we investigated the progression of xeno-GVHD responses in NSG-SGM3 hu-PBL models. We evaluated clinical symptoms, assessed T-cell responses induced by PBMCs collected from advanced-stage NSCLC patients, and compared these responses to those from HDs (23-25).

Our study identified significant differences in the presentation, onset, and kinetics of clinical responses associated with xeno-GVHD between NSCLC patients and HDs. The NSCLC patients models showed minimal to no signs of xeno-GVHD responses, indicating that their PBMCs might be less effective at initiating a rejection response than those from HDs.

T-cell subpopulation analysis conducted at various time points (4, 6, and 8 weeks post-PBMC injection) showed a

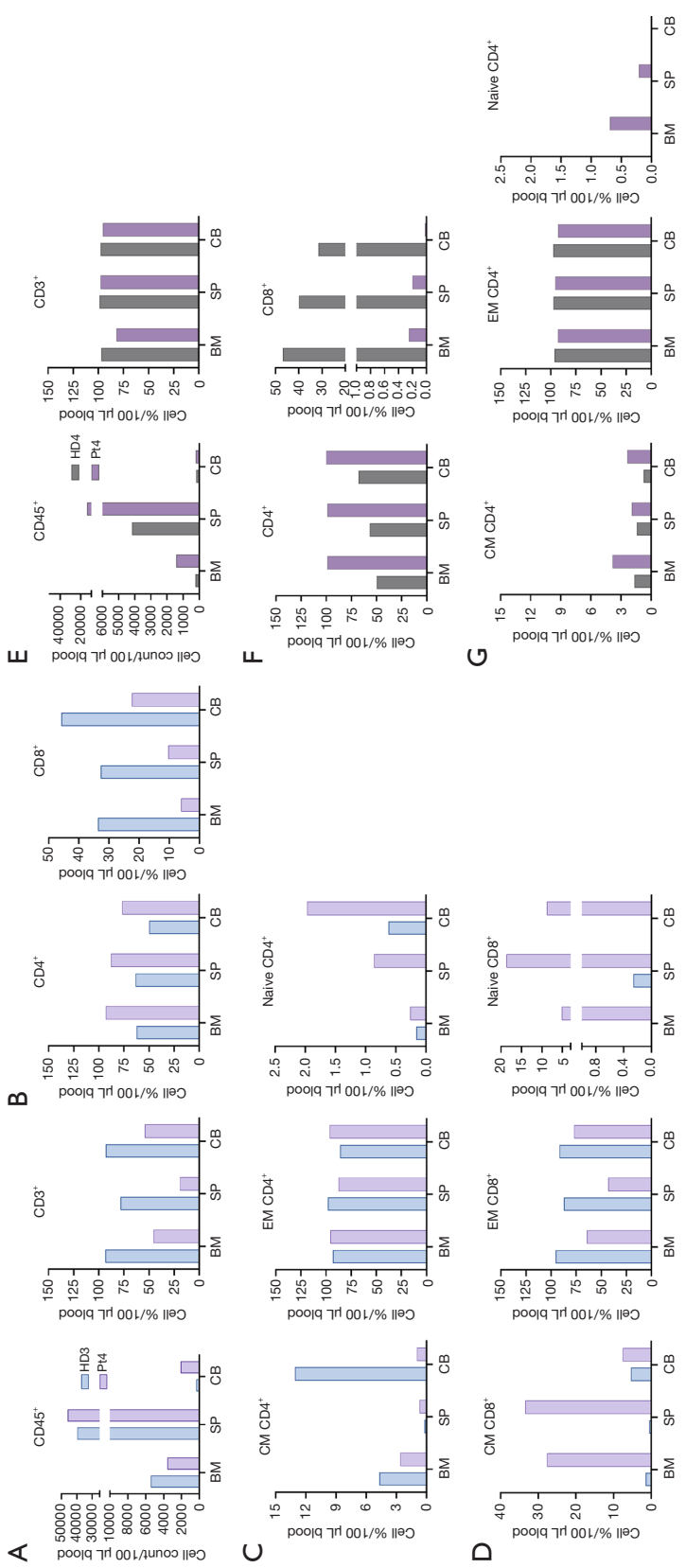

Figure 7 T-cell analysis from isolated mice organs of the hu-PBL model. PBMCs were collected from NSCLC patients and HDs and injected into NSG-SGM3 mice to create hu-PBL models. Flow cytometry analyzed T-cell compartments and subpopulations in various organs isolated from hu-PBL mice. Organs tested included BM, SP, and CB. Cellular analysis included $CD45^+$ cell count, $CD3^+$, CD4+ T cell, and $CD8^+$ T cell populations and subpopulations, CM, EM, and naive cells. (A-C) The outcomes for HD3 and Pt4 (mice, n=1), both of which developed severe xeno-GVHD and subsequently perished [HD3 (mouse M1) at week 4 and Pt4 (mouse M2) at week 6). (A) $CD45^+$ cell count and $CD3^+$ cell percentage. (B) $CD4^+$ and $CD8^+$ T-cells. (C) $CD4^+$ T cell subpopulation. (D) $CD8^+$ T-cell subpopulation. The color coding for this data is as follows: HD3 is light blue, and Pt4 is purple. (E-H) The findings for HD4 and Pt4, with one mouse per model. These mice did not exhibit a xeno-GVHD response and were euthanized in week 8. (E) $CD45^+$ cell count and $CD3^+$ cell percentage. (F) $CD4^+$ and $CD8^+$ T-cells. (G) $CD4^+$ subpopulation. (H) $CD8^+$ subpopulation. The color coding for these results is as follows: HD4 is grey, and Pt4 is purple. BM, bone marrow; CB, cord blood; CM, central memory; EM, effector memory; hu-PBL, human peripheral blood lymphocytes; HDs, healthy donors; NSCLC, non-small cell lung cancer; Pts, patients; SP, spleen; PBMCs, peripheral blood mononuclear cells; xeno-GVHD, xeno-graft versus host disease.

predominance of $CD8^+$ T cells in mice injected with PBMCs from HDs. This subset was primarily composed of EM T cells. In comparison, patients displayed a higher rate of $CD4^+$ T cells; however, EM T cells remained the dominant subtype in both groups. Additionally, mice injected with HD PBMCs consistently exhibited significantly higher counts of $CD45^+$ cells and elevated levels of $CD3^+$, CM, and EM $CD4^+$ T cells. Further assessment of T-cell kinetics over the various time points demonstrated that HDs could sustain higher levels of most T-cell subpopulations, except for the $CD4^+$ T-cell compartment, which was higher in the patients model. The higher levels of $CD4^+$ T cells in the patient model may be attributed to cancer-related immune dysregulation, chronic inflammation, or prior treatments, which can enhance $CD4^+$ T cell proliferation and persistence (27,28). In contrast, the higher levels of other T-cell subtypes in the HD model are likely due to an intact and diverse immune repertoire, with HDs having a more robust immune response compared to cancer patients, whose immune systems are often compromised by immune exhaustion and tumor-induced suppression (29).

Examination of mice's spleen, BM, and CB during advanced severe xeno-GVHD signs revealed an inverse ratio of CD4/CD8 cells, with a higher level of $CD4^+$ T cells in HD mice. However, a parallel distribution of T cell subpopulations persisted, with EM $CD4^+$ and $CD8^+$ T cells remaining the predominant subset. These findings align with previous studies that established $CD8^+$ T cells play a pivotal role in GVHD response induction through the IL-2 signaling pathway (26,30,31). The high level of $CD4^+$ T cells was previously reported and has been suggested to support the engraftment and expansion of the $CD8^+$ T cells during xeno-GVHD initiation (25,32). In consistence with our results, several works have demonstrated the transformation of human T-cells into an EM population (CD45RA–, CD197–) shortly after transplantation, with minimal detection of naïve T-cells (CD45RA+) (25,32,33). Additional work also showed a significant differentiation of $CD8^+$ memory T cells from $CD8^+$ naïve T cells during allo-GVHD (26). Notably, these memory T cells exhibited a pronounced ability to swiftly undergo proliferation and expansive growth, particularly in response to host dendritic cells, facilitated by the presence of IL-2, IL-7, and IL-15 (26). Interestingly, this EM T-cell phenotype was also identified after T-cell transplantation into MHC I and II depleted mouse models, which did not develop a xeno-GVHD response, suggesting that the reaction is not only antigen-driven but may be attributed to homeostatic proliferation, a phenomenon occurring in lymphopenic hosts such as NSG mice (25,34).

Analysis of Pt's clinical history indicated that the differences observed in our model between the manifestations of xeno-GVHD in patients and HDs PBMC-injected mice are likely contributed to T cell number levels and their proper functionality, which is interlinked to the treatment history of NSCLC patients, particularly chemotherapy. It was previously suggested that chemotherapeutic drugs exert direct cytotoxic effects on tumors and modulate the tumor immune microenvironment, impairing $CD8^+$ T-cell function (35-37). However, recent studies have highlighted that in various cancer types, chemotherapeutic agents can activate $CD8^+$ T cells in an MHC class I independent manner (36,38). Furthermore, studies have also indicated that the recovery of $CD8^+$ T cells may occur after chemotherapy treatment, contingent on multiple factors, including the patient's response to the therapy (38,39). These findings may explain the observed response of Pt4's PBMCs, which elicited the only xeno-GVHD reaction in the mouse model. All NSCLC patients in our study underwent treatment with immunotherapy, specifically immune checkpoint inhibitors (ICIs), which have emerged as a cornerstone in NSCLC care over the past decade (40,41). These treatments influence T-cell function by restoring it, thereby fostering a more potent antitumor immune response in patients (42,43). As such, ICI treatment history and response likely played a critical role in our study's induction time and absence of xeno-GVHD response in patients hu-PBL models. The delayed onset and absence of xeno-GVHD observed in NSCLC patients may also be attributed to T cell exhaustion. Recent investigations have focused on the role of the tumor microenvironment in resistance mechanisms in cancer patients, particularly those with LC (44,45). T-cell exhaustion is characterized by the sustained expression of inhibitory receptors and a diminished effector function, often resulting from chronic antigen exposure within the tumor microenvironment (44,45). This process has been linked to crucial markers, such as cytotoxic T-lymphocyte-associated protein 4 (CTLA-4), programmed cell death protein 1 (PD-1), and lymphocyte activation gene 3 (LAG-3).

Interestingly, Pt4, the only patient who induced a detectable and significant xeno-GVHD reaction, was diagnosed with advanced NSCLC adenocarcinoma and received a combination of cisplatin and Alimta for a single month in 2017, followed by continued treatment with nivolumab for a few years. At the time of the experiment, he

was on treatment with nivolumab as a single agent. While all four patients underwent chemotherapy, Pt4's treatment duration was the shortest and occurred several years ago (*Table 1*). ICI treatment in this patient showed effective results, indicating that his cells may have been activated due to the treatment. Further investigation is needed to understand how each treatment line and combination may impact the function of the T-cells and, consequently, the development and course of the xeno-GVHD reaction in NSCLC patients.

We chose the NSG-SGM3 mouse strain as the host for our hu-PBL model. Although this strain is less commonly used in solid tumor studies, it has demonstrated the ability to support a wider variety of human immune cells (19). This makes it an essential platform for understanding the interactions within the human immune system and the tumor microenvironment in a way that closely resembles human physiology (19,46,47). This feature provides a critically significant advantage in treatment selection studies in NSCLC (48), thus emphasizing the NSG-SGM3 model's potential to serve as a platform for developing robust and reliable humanized models advancing precision NSCLC treatment (19,25,46,47).

Despite our efforts, our study has several limitations, including a relatively small sample size, a narrow analysis of cellular components, and a need for more diversity in the clinical histories and demographics of the patients. Additionally, we could not conduct immunohistochemistry analysis or assess T cell exhaustion in additional organs affected during the xeno-GVHD response, which could have strengthened our findings. Nevertheless, our research provides valuable insights into the development and progression of xeno-GvHD responses induced by patients with advanced-stage NSCLC. We emphasize clinical factors that may influence a patient's suitability for using the hu-PBL model and enhance our understanding of immune system dynamics in the context of NSCLC patients. This contributes to the refinement and optimization of more reliable preclinical platforms.

Conclusions

This study reveals significant differences in xeno-GVHD progression between PBMCs from patients with advanced-stage NSCLC and HDs in NSG-SGM3 mice. We found that xeno-GVHD onset is delayed or absent, and its severity is reduced in hu-PBL models from NSCLC patients, likely due to changes from prior cancer treatments. These patients' altered functional state of T cells results in a unique xeno-GVHD phenotype, marked by varying T cell subpopulations influenced by individual clinical factors. These findings underline the importance of considering patients' immune profiles when using humanized mouse models for NSCLC research. Ultimately, our work enhances the relevance of hu-PBL models for evaluating NSCLC therapies and supports the development of personalized treatment strategies. Further research is needed to refine these models and better reflect the immune dynamics in NSCLC patients.

Acknowledgments

None.

Footnote

Reporting Checklist: The authors have completed the ARRIVE reporting checklist. Available at https://tlcr.amegroups.com/article/view/10.21037/tlcr-24-787/rc

Data Sharing Statement: Available at https://tlcr.amegroups.com/article/view/10.21037/tlcr-24-787/dss

Peer Review File: Available at https://tlcr.amegroups.com/article/view/10.21037/tlcr-24-787/prf

Funding: This study was partially supported by the BCRF foundation.

Conflicts of Interest: All authors have completed the ICMJE uniform disclosure form (available at https://tlcr.amegroups.com/article/view/10.21037/tlcr-24-787/coif). L.R. serves as an unpaid editorial board member of *Translational Lung Cancer Research* from February 2024 to January 2026. N.P. declares the following conflicts of interest: consulting fees and payment or honoraria for lectures, presentations, speakers bureaus, manuscript writing, or educational events from AstraZeneca, Bayer, Boehringer Ingelheim, Bristol-Myers Squibb, Eli Lilly, Imagine, Guardant360, Imagine, Merck, MSD, Novartis, Pfizer, Roche, and Takeda. Additionally, he has participated on Data Safety Monitoring Boards or Advisory Boards for these companies and holds stock or stock options in Imagine. The other authors have no conflicts of interest to declare.

Ethical Statement: The authors are accountable for all

aspects of the work in ensuring that questions related to the accuracy or integrity of any part of the work are appropriately investigated and resolved. Experiments were performed under a project license (No. IL-59-11-2018) granted by the Institutional Animal Care and Use Committee of Ben Gurion University (BGU), in compliance with Israel Ministry of Health (MOH) national or institutional guidelines for the care and use of animals. The study was conducted in accordance with the Declaration of Helsinki (as revised in 2013). The ethics committee of Soroka Medical Center (No. 0026-19-SOR) approved the study. Informed consent was obtained from all subjects and their legal guardians.

References

1. Leiter A, Veluswamy RR, Wisnivesky JP. The global burden of lung cancer: current status and future trends. Nat Rev Clin Oncol 2023;20:624-39.
2. Chalela R, Curull V, Enríquez C, et al. Lung adenocarcinoma: from molecular basis to genome-guided therapy and immunotherapy. J Thorac Dis 2017;9:2142-58.
3. Kumari R, Feuer G, Bourré L. Humanized Mouse Models for Immuno-oncology Drug Discovery. Curr Protoc 2023;3:e852.
4. Chuprin J, Buettner H, Seedhom MO, et al. Humanized mouse models for immuno-oncology research. Nat Rev Clin Oncol 2023;20:192-206.
5. De La Rochere P, Guil-Luna S, Decaudin D, et al. Humanized Mice for the Study of Immuno-Oncology. Trends Immunol 2018;39:748-63.
6. Tian H, Lyu Y, Yang YG, et al. Humanized Rodent Models for Cancer Research. Front Oncol 2020;10:1696.
7. Chen A, Neuwirth I, Herndler-Brandstetter D. Modeling the Tumor Microenvironment and Cancer Immunotherapy in Next-Generation Humanized Mice. Cancers (Basel) 2023;15:2989.
8. Yin L, Wang XJ, Chen DX, et al. Humanized mouse model: a review on preclinical applications for cancer immunotherapy. Am J Cancer Res 2020;10:4568-84.
9. Wang M, Yao LC, Cheng M, et al. Humanized mice in studying efficacy and mechanisms of PD-1-targeted cancer immunotherapy. FASEB J 2018;32:1537-49.
10. Wang M, Herbst RS, Boshoff C. Toward personalized treatment approaches for non-small-cell lung cancer. Nat Med 2021;27:1345-56.
11. Bareham B, Georgakopoulos N, Matas-Céspedes A, et al. Modeling human tumor-immune environments in vivo for the preclinical assessment of immunotherapies. Cancer Immunol Immunother 2021;70:2737-50.
12. Pyo KH, Kim JH, Lee JM, et al. Promising preclinical platform for evaluation of immuno-oncology drugs using Hu-PBL-NSG lung cancer models. Lung Cancer 2019;127:112-21.
13. Brehm MA, Shultz LD, Luban J, et al. Overcoming current limitations in humanized mouse research. J Infect Dis 2013;208 Suppl 2:S125-30.
14. Sanmamed MF, Chester C, Melero I, et al. Defining the optimal murine models to investigate immune checkpoint blockers and their combination with other immunotherapies. Ann Oncol 2016;27:1190-8.
15. Huang F, Cao FL, Zheng SG. Update of humanized animal disease models in studying Graft-versus-host disease. Hum Vaccin Immunother 2018;14:2618-23.
16. King MA, Covassin L, Brehm MA, et al. Human peripheral blood leucocyte non-obese diabetic-severe combined immunodeficiency interleukin-2 receptor gamma chain gene mouse model of xenogeneic graft-versus-host-like disease and the role of host major histocompatibility complex. Clin Exp Immunol 2009;157:104-18.
17. Brehm MA, Kenney LL, Wiles MV, et al. Lack of acute xenogeneic graft- versus-host disease, but retention of T-cell function following engraftment of human peripheral blood mononuclear cells in NSG mice deficient in MHC class I and II expression. FASEB J 2019;33:3137-51.
18. Covassin L, Jangalwe S, Jouvet N, et al. Human immune system development and survival of non-obese diabetic (NOD)-scid IL2rγ(null) (NSG) mice engrafted with human thymus and autologous haematopoietic stem cells. Clin Exp Immunol 2013;174:372-88.
19. Yao LC, Cheng M, Aryee KE, et al. Abstract 5676: Patient-derived tumor xenografts in humanized NSG-SGM3 mice: An improved immuno-oncology platform. Cancer Res 2018;78:5676.
20. Haque M, Boardman DA, Lam AJ, et al. Modelling Graft-Versus-Host Disease in Mice Using Human Peripheral

Blood Mononuclear Cells. Bio Protoc 2022;12:e4566.
21. Bray F, Ferlay J, Soerjomataram I, et al. Global cancer statistics 2018: GLOBOCAN estimates of incidence and mortality worldwide for 36 cancers in 185 countries. CA Cancer J Clin 2018;68:394-424.
22. Casal-Mouriño A, Ruano-Ravina A, Lorenzo-González M, et al. Epidemiology of stage III lung cancer: frequency, diagnostic characteristics, and survival. Transl Lung Cancer Res 2021;10:506-18.
23. Verma B, Wesa A. Establishment of Humanized Mice from Peripheral Blood Mononuclear Cells or Cord Blood CD34+ Hematopoietic Stem Cells for Immune-Oncology Studies Evaluating New Therapeutic Agents. Curr Protoc Pharmacol 2020;89:e77.
24. Ehx G, Somja J, Warnatz HJ, et al. Xenogeneic Graft-Versus-Host Disease in Humanized NSG and NSG-HLA-A2/HHD Mice. Front Immunol 2018;9:1943.
25. Hess NJ, Brown ME, Capitini CM. GVHD Pathogenesis, Prevention and Treatment: Lessons From Humanized Mouse Transplant Models. Front Immunol 2021;12:723544.
26. Zhang Y, Joe G, Hexner E, et al. Alloreactive memory T cells are responsible for the persistence of graft-versus-host disease. J Immunol 2005;174:3051-8.
27. Coussens LM, Werb Z. Inflammation and cancer. Nature 2002;420:860-7.
28. Fridman WH, Zitvogel L, Sautès-Fridman C, et al. The immune contexture in cancer prognosis and treatment. Nat Rev Clin Oncol 2017;14:717-34.
29. Ostrand-Rosenberg S, Sinha P. Myeloid-derived suppressor cells: linking inflammation and cancer. J Immunol 2009;182:4499-506.
30. Cho JH, Kim HO, Kim KS, et al. Unique features of naive CD8+ T cell activation by IL-2. J Immunol 2013;191:5559-73.
31. Jiang H, Fu D, Bidgoli A, et al. T Cell Subsets in Graft Versus Host Disease and Graft Versus Tumor. Front Immunol 2021;12:761448.
32. Ito R, Katano I, Kawai K, et al. A Novel Xenogeneic Graft-Versus-Host Disease Model for Investigating the Pathological Role of Human CD4(+) or CD8(+) T Cells Using Immunodeficient NOG Mice. Am J Transplant 2017;17:1216-28.
33. Ali N, Flutter B, Sanchez Rodriguez R, et al. Xenogeneic graft-versus-host-disease in NOD-scid IL-2Rγnull mice display a T-effector memory phenotype. PLoS One 2012;7:e44219.
34. Zumwalde NA, Gumperz JE. Modeling Human Antitumor Responses In Vivo Using Umbilical Cord Blood-Engrafted Mice. Front Immunol 2018;9:54.
35. Maeda K, Hazama S, Tokuno K, et al. Impact of chemotherapy for colorectal cancer on regulatory T-cells and tumor immunity. Anticancer Res 2011;31:4569-74.
36. van der Most RG, Currie AJ, Cleaver AL, et al. Cyclophosphamide chemotherapy sensitizes tumor cells to TRAIL-dependent CD8 T cell-mediated immune attack resulting in suppression of tumor growth. PLoS One 2009;4:e6982.
37. Chen C, Chen Z, Chen D, et al. Suppressive effects of gemcitabine plus cisplatin chemotherapy on regulatory T cells in nonsmall-cell lung cancer. J Int Med Res 2015;43:180-7.
38. Knaus HA, Berglund S, Hackl H, et al. Signatures of CD8+ T cell dysfunction in AML patients and their reversibility with response to chemotherapy. JCI Insight 2018;3:e120974.
39. Coleman S, Clayton A, Mason MD, et al. Recovery of CD8+ T-cell function during systemic chemotherapy in advanced ovarian cancer. Cancer Res 2005;65:7000-6.
40. Marin-Acevedo JA, Kimbrough EO, Lou Y. Next generation of immune checkpoint inhibitors and beyond. J Hematol Oncol 2021;14:45.
41. Darvin P, Toor SM, Sasidharan Nair V, et al. Immune checkpoint inhibitors: recent progress and potential biomarkers. Exp Mol Med 2018;50:1-11.
42. Nagano T, Tachihara M, Nishimura Y. Molecular Mechanisms and Targeted Therapies Including Immunotherapy for Non-Small Cell Lung Cancer. Curr Cancer Drug Targets 2019;19:595-630.
43. Steven A, Fisher SA, Robinson BW. Immunotherapy for lung cancer. Respirology 2016;21:821-33.
44. Kim CG, Kim G, Kim KH, et al. Distinct exhaustion features of T lymphocytes shape the tumor-immune microenvironment with therapeutic implication in patients with non-small-cell lung cancer. J Immunother Cancer 2021;9:e002780.
45. Zhou H, Liu T, Wang Z. Analysis of non-small cell lung cancer microenvironment indicates preponderance of T cell exhaustion marker expression. Exp Cell Res 2017;360:205-9.
46. Ye C, Brehm M, Cheng M, Shultz L, et al. Abstract 3902: Increased sensitivity for detecting cytokine release syndrome with cancer immunotherapy using a PBMC humanized NSG-SGM3 mouse model. Cancer Res 2019;79:3902.
47. Yao LC, Aryee KE, Cheng M, et al. Creation of PDX-

Bearing Humanized Mice to Study Immuno-oncology. Methods Mol Biol 2019;1953:241-52.
48. Lin A, Wei T, Meng H, et al. Role of the dynamic tumor microenvironment in controversies regarding immune checkpoint inhibitors for the treatment of non-small cell lung cancer (NSCLC) with EGFR mutations. Mol Cancer 2019;18:139.

Cite this article as: Fuchs V, Roisman L, Msamra M, Refaely Y, Cohen AY, Porgador A, Peled N, Sobarzo A. Characterization of the xeno-GVHD response generated by advanced lung cancer patient peripheral blood mononuclear cells in NSG-SGM3 mice. Transl Lung Cancer Res 2025;14(4):1301-1319. doi: 10.21037/tlcr-24-787